

ARTICLE OPEN



Antimicrobial enhancement via Cerium (II)/Lanthanum (III)-doped TiO₂ for emergency leak sealing polyurea coating system

Yuanzhe Li¹, Cong Fang², Wei-Qin Zhuang³, Haojing Wang⁴ and Xueli Wang^{5,6}✉

Industrial piping structures often suffer from corrosion caused by biofouling or chemical etching, which can cause immediate structural failure. Polyurea coatings, which are fabricated for emergency leak sealing, are able to form high mechanical strength coating surfaces within seconds. After its further modification via Ce/La-doped TiO₂, the polyurea coating will indicate an increment in mechanical strength, chemical durability, and reduction of microbial attachment. Due to the adsorption by the Ce/La-doped TiO₂ and generation of reactive oxygen species (ROS), *E. coli* and *Pseudomonas* may lose their living conditions during the progress, and planktonic bacteria cells are prevented from enriching on the surface. The Ce/La-dopants can also improve the original photocatalytic response of nano-TiO₂ to UV light and environmental temperature. These Ce/La-doped TiO₂ polyurea coatings illustrate an immediate application for emergency leak sealing purposes without any production interruption and it may prolong the time intervals for the maintenance service as well.

npj Materials Degradation (2022)6:41 ; <https://doi.org/10.1038/s41529-022-00249-x>

INTRODUCTION

The semiconductor manufacturing process constantly generates harmful gases, and it is requested to be properly treated before ventilated into the exhaust pipes or released into the air^{1,2}. These piping systems are often suffered from biological and chemical corruptions, which can increase the flow resistance in the associated units such as scrubbers and exhaust systems³. Severe biological or chemical corruptions can even cause structural failure and skyrocket the cost of maintenance. Therefore, the semiconductor industry needs a rapid surface coating technology that can prevent the development of corruptions on the original surfaces without alternating the surface properties or interrupting the manufacturing process. Thus, a durable and stretchable emergency leak sealing coating system is developed in this study. Additional properties, such as antibiofouling, self-healing, drag reduction, chemical durability, and fire retardancy, of this coating system make it very appealing to the semiconductor industry⁴.

Polymer composite materials with multi functionalities have been increasingly used in different fields such as aerospace, automotive, sports, and healthcare with enhanced performance⁵. With the advances in chemistry and materials, multifunctional materials will provide a sustainable, environmentally friendly, and pervasive solution to manufacturing industry⁶. There are numerous biological mechanisms for those polymer materials that can inhibit or prevent bacteria colonization on solid surfaces, including non-specific inhibition (e.g., anti-adhesive polymers) and specific inhibition via disrupting signalling pathways, enzymatic action on EPS matrix, and destruction of bacteria persisters⁷. In contrast, chemical durable coatings are often made up of hydrophobic nanofillers or functional monomers to enhance water resistance⁸, e.g., inorganic nanomaterials silica sol composite blending copolymerization modification method, etc.

Two components of elastomeric polyurea coating have recently received attentions as emergency leak sealants due to their unique characteristics such as fast curing, chemical resistance to a broad range of corrosives and solvents, outstanding thermomechanical properties, and anti-abrasive properties. In previous research, titania-polyurea (TiO₂-SPUA) coatings were reported to reduce the biofilm attachment in the marine field test⁸. Moreover, such TiO₂-SPUA coating system is fire-resistant, thus, can be long-term used under 393 K. Through our preliminary studies, it is believed that the introduction of limited amount of rare-earth (RE) elements to nano-TiO₂ is able to further improve its original photocatalytic activity by prolonging the recombination time in between electron and hole^{7,8}. The RE-elements may absorb and emit electromagnetic wave radiation of a wider wavelength range than the ultraviolet region^{9–11}.

In this paper, the Cerium (II)/Lanthanum (III) (Ce/La)-doped anatase nano-TiO₂ polyurea coatings with enhanced antimicrobial performance is obtained via blending preparation. The antibacterial activities with different environmental temperature and light exposure, and chemical durability and robustness are also investigated in the study. The results indicate its great potential in the emergency leak sealing coating system for industrial piping response and protective actions^{12,13}.

RESULTS AND DISCUSSION

X-ray diffraction analysis

X-ray diffraction (XRD) graphs, as shown in Fig. 1, removed the specific absorption bands of Pure_polyurea to indicate the undoped nano-TiO₂ and Ce/La-dopants, and the diffraction peaks of Ce/La-doped nano-TiO₂ polyurea coating samples were the standard values of tetragonal nano-TiO₂ obtained from the

¹School of Materials Science & Engineering, Nanyang Technological University, Singapore 639798, Singapore. ²School of Software Technology, Zhejiang University, Hangzhou 310058, China. ³School of Civil and Environmental Engineering, University of Auckland, Auckland 1010, New Zealand. ⁴School of Chemical and Biomedical Engineering Nanyang Technological University, Singapore 639798, Singapore. ⁵Institute of Central China Development, Wuhan University, Wuhan 430072, China. ⁶Department of Geography, National University of Singapore, 1 Arts Link, 117570 Singapore, Singapore. ✉email: sherrywang@whu.edu.cn

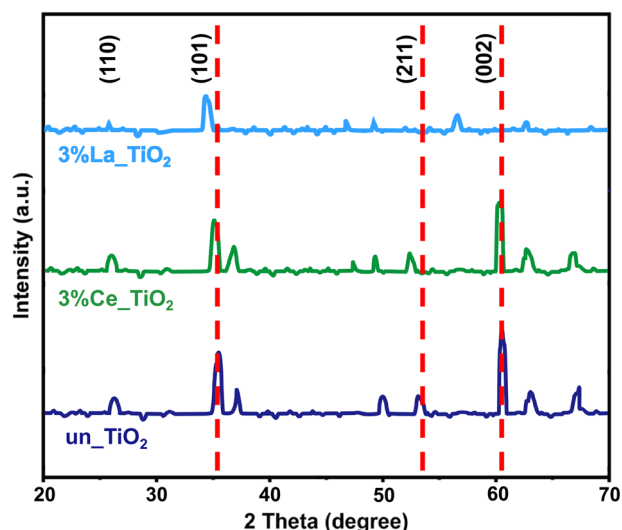


Fig. 1 XRD patterns of un_TiO₂, 3%Ce_doped TiO₂, and 3%La_doped TiO₂ polyurea coatings. The diffraction peaks of Ce/La-doped nano-TiO₂ at 2θ has shifted towards lower angles compared to the nano-TiO₂ (1 0 1) at $2\theta = 36.28^\circ$, which was due to the larger radius of Ce/La-dopants ($\text{Ce}^{3+} = 1.02 \text{ \AA}$ and $\text{La}^{3+} = 0.96 \text{ \AA}$) than that of Ti (0.60 \AA).

literature. Refined structural parameters of tetragonal nano-TiO₂ at 300 K are as follows: the lattice constants and unit cell volume are $a = b = 3.78 \text{ \AA}$, $c = 9.49 \text{ \AA}$ and $V = 136.43 \text{ \AA}^3$, respectively¹⁴. The XRD patterns of the undoped nano-TiO₂ and Ce/La-doped nano-TiO₂ revealed the presence of nano-TiO₂ exclusively in an anatase phase after thermal annealing. No impurity peaks of La (La^{3+}) cluster or La_2O_3 , Ce (Ce^{3+}) cluster, or Ce_2O_3 were observed¹⁵. However, the intensity of the original diffraction peaks decreased with the introduction of Ce/La-dopants, indicating a loss of crystallinity due to lattice distortion. The diffraction peaks of those Ce/La-doped nano-TiO₂ at 2θ has shifted towards lower angles compared to the nano-TiO₂ (1 0 1) at $2\theta = 36.28^\circ$, which was due to the larger radius of Ce/La-dopants ($\text{Ce}^{3+} = 1.02 \text{ \AA}$ and $\text{La}^{3+} = 0.96 \text{ \AA}$) than that of Ti (0.60 \AA)¹⁶. The peaks for polyurea coating with nano-TiO₂ and Ce/La-doped nano-TiO₂ groups had slight differences, indicating that the crystallographic positions of Ce/La-dopant ions were successfully occupied in the TiO₂ host lattice and strain developed in the lattice. Besides, the alignment of the polyurea chain remained regular and uniform even after the introduction of the undoped TiO₂ and Ce/La-doped TiO₂¹⁷, which could guarantee the good adhesion force between those nanoparticles and the polyurea coating systems.

In general, when Ce/La-dopants were incorporated into the periodic crystal lattice of nano-TiO₂, a strain might also be induced into the system, resulting in the alteration of the lattice periodicity and a decrease in crystal symmetry¹⁸. It was also noted that polyurea coating with Ce/La-doped TiO₂ indicated a shift towards lower the value compared to the coating with un-doped TiO₂ due to the incorporation of Ce/La-oxides into nano-TiO₂. Furthermore, there were no other peaks of impurities detected in the XRD patterns of these coating samples.

SEM and TEM characterizations

Figure 2a, d showed the surface morphology of polyurea coatings with (a) Pure_polyurea, with (b) un_TiO₂, (c) 3% Ce-doped TiO₂, and (d) 3% La-doped TiO₂ polyurea coatings respectively. Most of the coating samples would exhibit similarly flat surface morphology. After the introduction of undoped nano-TiO₂ and Ce/La-doped nano-TiO₂ into the polyurea coating sample, the coatings indicated micro-scale convex structures with $1.5\text{--}5.8 \mu\text{m}$ of

diameters randomly oriented and aggregated on their surfaces, which might be the platelets of the nano-TiO₂ or Ce/La-doped nano-TiO₂⁸. And the rare elements were able to be observed in energy dispersive spectrometer (EDS) mappings in Fig. 2 as well. Moreover, the samples with Ce/La-doped nano-TiO₂ as shown in Fig. 2c, d would exhibit even clearer surface textures and relatively deeper surface roughness, which might also influence the wettability performance, would be discussed in detail in the following chapters.

Figure 3a, d indicated the correspondent transmission electron microscopy (TEM) imaging of polyurea coatings using LaB6 electron source. High resolution spectra were collected using 25 eV at 0.1 eV steps with a chamber pressure below 7.5×10^{-9} mbar¹⁸. Images were taken at a working distance of 7 mm and a potential of 5 kV. Ce/La-doped nano-TiO₂ polyurea coating was observed with a tetragonal crystal shape as shown in Fig. 3c, d. This observation was in agreement with the TEM imaging of Cerium and Lanthanum oxides (CeO_2 and La_2O_3) during the synthesis process of Ce/La-doped nano-TiO₂^{19,20}. And all TEM micrographs for these polyurea coatings with Ce/La-doped nano-TiO₂ still revealed similar micro-structures as those with undoped TiO₂²¹.

Physico-mechanical properties of Ce/La-doped TiO₂-polyurea coating

The physico-mechanical properties of polyurea coatings are important parameters that determine their applications as emergency leak sealing coating. Lower mechanical properties mean the materials are prone to be destructed by internal and external forces. The dimensions of the length and width of specimens were 9.53 mm and 3.18 mm respectively. The tensile and flexural properties of the nanocomposites were measured by AGS-J (SHIMADZU/SSL, Shanghai, China). The tests were performed as per ASTM: D638 and ASTM: D790-10 methods, respectively^{22,23}. A cylindrical cutter with inner diameter of 6 mm compressed with a hydronic compressor via the same equipment was used to prepare specimens for compression tests. ASTM-D-2240-00 Type A Teclock durometer (Shenzhen, China) was used to test the hardness and its impact resistance and durability²⁴. The tensile, compression, flexural strength and surface hardness test results are listed in Table 1. The loading of undoped and Ce/La-doped nano-TiO₂ significantly increased the strain performance. The higher the failure strain, the better the crack resistance of the coating when the coating sample was bent.

The tensile test results showed that the tested specimens did not exhibit obvious fracture at a high strain rate, which was set as high as 500%. With continuously increasing strain rate, the coating samples went on initial microcracks and then fractured into two pieces. It indicated that the 3%La_TiO₂ had a slightly higher tensile strength than 3%Ce_TiO₂ or un_TiO₂, which might be attributed to the well-structured La-dopants and flexural tests. The proper amount of the undoped and Ce/La-doped TiO₂ within the polyurea coating exhibited binding characters bridging the crack surfaces and retained the integrity of coatings, which underwent considerable deformation when the tensile stress acted. The increase of the tensile strength might also align with flexural strength for all the coating samples with nano-TiO₂.

The hardness results revealed that the introduction of the TiO₂ nanoparticles had significantly increased the shore hardness from 39 A to 71 A. Moreover, the compression behaviour was consistent with the hardness test. The 3%La_TiO₂ took the lead in the shore hardness test at 72 A, and the compression test at 29.7 MPa⁷. One more thing that needed to be noted was that there was no significant yield failure in the compression and flexural test for all groups of polyurea coating specimens, which indicated the high mechanical performance for the polyurea itself. In addition, the less touch-dry curing time of un_TiO₂, 3% Ce_TiO₂, and 3%

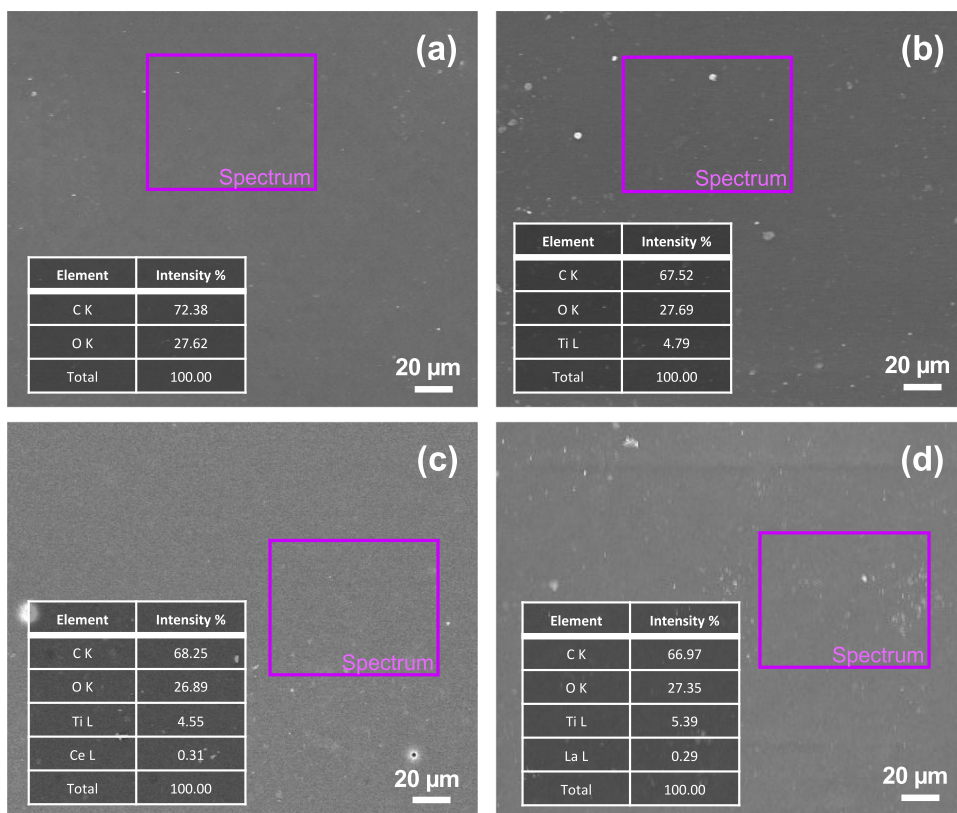


Fig. 2 SEM micrographs. **a** Pure polyurea, with **b** undoped TiO₂, **c** 3%Ce-doped TiO₂, and **d** 3%La-doped TiO₂ polyurea coatings. After the introduction of undoped nano-TiO₂ and Ce/La-doped nano-TiO₂ into the polyurea coating sample, the coatings indicated micro-scale convex structures with 1.5–5.8 μm of diameters randomly oriented and aggregated on their surfaces.

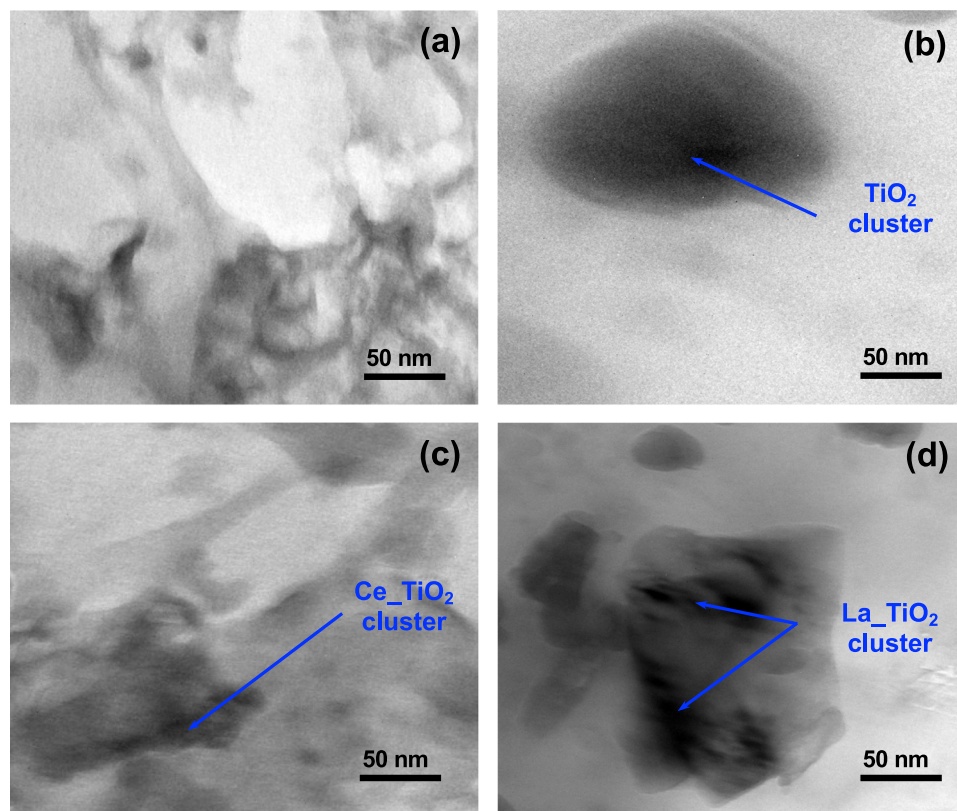






Fig. 3 TEM micrographs. **a** Pure polyurea, with **b** un-TiO₂, **c** 3%Ce-doped TiO₂, and **d** 3%La-doped TiO₂ polyurea coatings. Ce/La-doped nano-TiO₂ polyurea coating was observed with a tetragonal crystal shape.

Table 1. Effect of Ce/La-doped TiO₂ on physico-mechanical properties of polyurea.

Formula No.	Curing Time/min	Tensile Strength/MPa	Compression Stress/MPa	Flexural strength/MPa	Shore Hardness/A
Pure_polyurea	2.0 ± 0.5	12.5 ± 1.2	16.5 ± 0.2	23.4 ± 1.5	39 ± 2.1
un_TiO ₂	1.5 ± 0.8	17.9 ± 0.9	18.6 ± 0.7	23.7 ± 1.7	71 ± 1.9
3% Ce_TiO ₂	1.0 ± 0.4	18.3 ± 0.4	28.6 ± 1.0	24.1 ± 1.2	70 ± 2.2
3% La_TiO ₂	1.2 ± 0.3	18.4 ± 1.1	29.7 ± 0.8	23.8 ± 1.5	72 ± 1.7

Table 2. Values (Mean ± SD) of Surface Roughness (Ra), Contact Angle (CA) and Surface Energy (SFE).

	Surface roughness (R _a mean)/μm	Contact angle (CA)/deg	Surface Energy (SFE)/mJ/m ²	Contact angle image
Pure_polyurea	0.19 ± 0.04	40.5 ± 1.7	52.3	
un_TiO₂	0.36 ± 0.07	64.4 ± 1.9	37.2	
3%Ce-doped TiO₂	0.45 ± 0.10	68.4 ± 2.4	32.5	
3%La-doped TiO₂	0.47 ± 0.09	71.0 ± 2.1	32.5	

La-TiO₂ proved their great potentials for the application as an emergency leak seal coating compared to Pure-polyurea. These physico-mechanical properties might also become a great reference for the optimization works for the formula design.

Surface wettability and chemical durability

Surface wettability and surface energy. The test results of surface roughness (R_a), contact angle (CA), and surface energy (SFE) were summarized in Table 2. The Pure_polyurea coatings indicated a relatively flat surface character with 0.19 ± 0.04 μm with CA = 40.5 deg and SFE = 52.3 mJ m⁻². However, after introducing undoped nano-TiO₂ or Ce/La doped TiO₂, the surface roughness became higher and for both 3%Ce-doped TiO₂ and 3%La-doped TiO₂ coatings. This microstructure could be observed in the morphology analysis as listed in the second column of Table 2, which might also change the polar component of the coating surface since the dispersive part remained constant. And such R_a increment caused by the regular distribution of Ce/La doped TiO₂ might also contribute to the increase of contact angle and the reduction of the surface energy. Besides, both pure undoped TiO₂ and Ce/La dopants would normally perform as super hydrophilic wettability according to the literature citations, while the actual contact angle results for all three doped polyurea coatings were opposed the conclusion. This was due to the small amount of defoamer agent, polydimethylsiloxane (PDMS), during the polyurea preparation⁷. Recently, other groups of other rare-earth (RE) additives underwent the biofilm assays and CA & SFE characterization test, and the range of optimized mass weight of dopants was suggested to be within 2.5–4.0 wt.% of the total prescription. Furthermore, as the weight percentage of these nanoparticles continuously went higher, the nano-surface texture would gradually disappear, and hydrophilic character would take the lead in the series experiments.

Surface chemical durability. Chemical durability was also an important characteristic performance for emergency leak sealing coatings. Due to the high concentration of chemicals, electrochemical corrosion, and air-oxidation reaction inside the wet scrubber system, many traditional emergency leak sealing coatings might lose their hydrophobicity or texture structures. The peeling-off of

those coatings and the corrosion of the original metal-based pipe might seriously affect their applications and even the production^{3,4,8}. Hence, a long-period immersion in acid, alkaline and saline solution to test the chemical durability is also important for the characteristic performance of polyurea coatings.

As shown in Fig. 4, after continuous immersion for 50 days and measuring the contact angle every 5 days, all polyurea coatings indicated outstanding chemical durability in 8.0% hydrochloric acid (Fig. 4a), sodium hydroxide (Fig. 4b), and saline water (Fig. 4c) respectively. The contact angle and hydrophilic wettability of all polyurea groups indicated a slight reduction within the range of ±8.0 deg even after 50-day exposure. In other words, this coating platform could maintain relatively long-term stability in different chemical environments. In addition, the results for un_TiO₂, 3%Ce-doped TiO₂, and 3%La-doped TiO₂ polyurea coatings indicated a bit different after 20 days of chemical immersions. The un_TiO₂ polyurea coating demonstrated a continuous decrease in alkaline and saline water solutions, whereas the 3%Ce-doped TiO₂, and 3%La-doped TiO₂ polyurea coatings remained stable at around 68 ± 3.0 deg. The mechanism of the chemical durability was mostly due to the material characteristics and micro-nano roughness of the Ce/La-doped TiO₂ surface of the polyurea coating. If the surface structure is not changed, it will not affect the hydrophilicity of the polyurea coating itself at all.

UV-Vis diffuse reflectance spectra analysis

The introduction of undoped nano-TiO₂ and Ce/La-doped nano-TiO₂ in polyurea coatings played an important role in optical and photocatalytic activities¹⁸. The absorption spectra of nano-TiO₂ and Ce/La-doped nano-TiO₂ was indicated in Fig. 5. The spectra of the nano-TiO₂ only exhibited a strong absorption band at about 242 nm²⁵. Due to the band-gap transition from the valence band (VB) to the conduction band (CB) of the pure nano-TiO₂, the samples with nano-TiO₂ had the same band-gap transition at about 421 nm (3.2 eV). However, the use of different Ce/La-doped nano-TiO₂ dopants did not change the absorption band of the polyurea coatings. The trend for all Ce/La-doped nano-TiO₂ samples closely approximated the undoped nano-TiO₂ coating group, indicating that the Ce/La-dopants in the nano-TiO₂ matrix did not affect its original transition directly²¹.

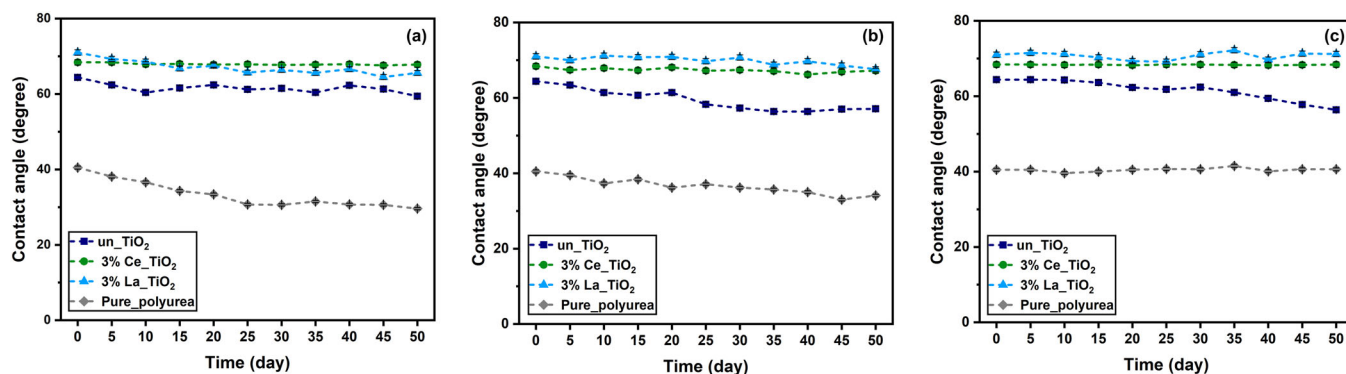


Fig. 4 Surface wettability variability for continuous 50 days in three different chemicals. **a** Hydrochloric acid (acid), **b** sodium hydroxide (alkaline), and **c** sodium chloride (saline) solution.

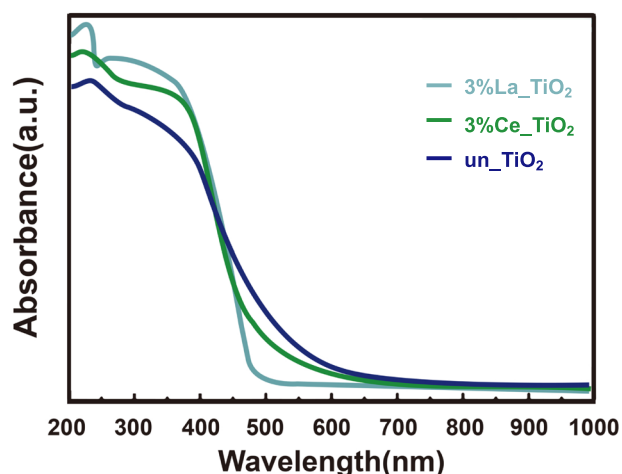


Fig. 5 UV-Vis absorption spectra of un_TiO₂, 3%Ce-doped TiO₂, and 3%La-doped TiO₂. Ce/La-dopants may improve the photon utilization and enhance the photocatalytic activity of nano-TiO₂.

In the case of coating with 3%La-doped TiO₂, a slightly wider wavelength range and higher absorbance were detected even at the same wavelength after comparing with other dopant groups, demonstrating its outstanding photocatalytic properties²⁰. Lanthanum (La) has a complex energy level structure, and the doping of La dopants into nano-TiO₂ would introduce new impurity energy levels in its forbidden band, lower the bandgap energy, and expand the response range of the TiO₂ absorption spectrum. Other than 3%La-doped TiO₂, the presence of 3%Ce-doped TiO₂ could also promote interfacial charge transfer and inhibit the complexation of photogenerated electron-hole pairs. When nano-TiO₂ was photoexcited and generated electrons, the Ce-dopants at the interstitial position could effectively trap them and make them react with the O₂ molecules to generate superoxide ion radicals ($\cdot\text{O}_2^-$).

Thus, both Ce/La-dopants might improve the photon utilization and enhance the photocatalytic activity of nano-TiO₂. However, once the doping of Ce/La-dopants became too much, it would again become the compound centre of the electron-hole pair, accelerating the electron-hole compound, but inhibiting the photocatalytic performance of nano-TiO₂. Finally, for all the RE-doped nano-TiO₂ coatings, they all contained a small overlap of absorption extending with the visible region, which provided indirect evidence for the Ce/La-doped nano-TiO₂ polyurea coating sample obtaining the outstanding bactericidal activities in the following sections even under poor light exposure level^{8,19}.

Antibacterial activity analysis

LIVE/DEAD biofilm imaging. Figure 6 and 7 indicated 20 min treatment for the four polyurea coating coupons under 308 K. Both LIVE and DEAD imaging of bacteria cells were captured from these groups. DEAD or dying cells with compromised membranes would be stained brightly red, whereas the LIVE cells with an intact membrane would be stained brightly green. However, as the coupons with *Pseudomonas* attachment had a strong autofluorescence signal from the Syto9 wavelength, LIVE and Dead cells of *Pseudomonas* were captured separately. Whereas the LIVE and Dead *E. coli* could be captured within the same image.

In Fig. 6a, h, significant LIVE *Pseudomonas* could be observed at Pure_polyurea coating samples with obvious green signage. The undoped nano-TiO₂, 3%Ce-doped TiO₂, and 3%La-doped TiO₂ remained clear after the long-time exposure of *Pseudomonas*, which proved their antibacterial effect for cells. The DEAD biofilm imaging of *Pseudomonas* demonstrated a slight autofluorescence effect. However, it could be still observed that the cell structures of *Pseudomonas* were already broken, as the leaking DNA was clearly stained, after it was exposed to the undoped nano-TiO₂, 3% Ce-doped TiO₂, and 3%La-doped TiO₂ samples. Compared with the undoped TiO₂ samples, the Ce/La-doped TiO₂ samples demonstrated clearer signage of the broken cells, which might be due to its potential thermal catalytic character under high temperatures. Moreover, the surface textures might also contribute to the less attachment of both bacteria, which was discussed in the following chapter regarding their surface wettability. Zeta Potential test was also conducted for the leaching test of particles every time the coupons taken out and withdrawn from the CDC reactor^{26,27}. The result was that there was no obvious reading within both fresh and waste carboy, which could be considered as a limited impact of Ce/La-doped TiO₂ on the environment.

In Fig. 7, DEAD *E. coli* cells could be more obviously characterized for all the coating coupons. The Pure_polyurea coating illustrated fewer dead or dying cells than any other polyurea coating samples with nano-TiO₂ or Ce/La-doped TiO₂. One more thing that might be needed to note was that the flat Pure_polyurea coating surface might reduce the possibility of the initial adhesion of the planktonic *E. coli* cells as in Fig. 7a. At the same time, undoped un_TiO₂, 3% Ce-doped TiO₂, and 3%La-doped TiO₂ coupons indicated more stained red dye, due to their higher surface roughness and surface fluid convection factors, which indicated more the dead cells accumulated on the concave portion of the coating surface as shown in Fig. 7b, c, d. Moreover, the elimination of the *E. coli* cells would highly depend on the near-wall photocatalytic effect/photodegradation for the nano-TiO₂ group, and there might be a higher concentration of near-wall reactive oxygen species (ROS) for Ce/La-doped TiO₂ groups than with simple nano-TiO₂ groups²⁷. Hence more small pieces of *E. coli* broken cell structures enriching on the surface could be

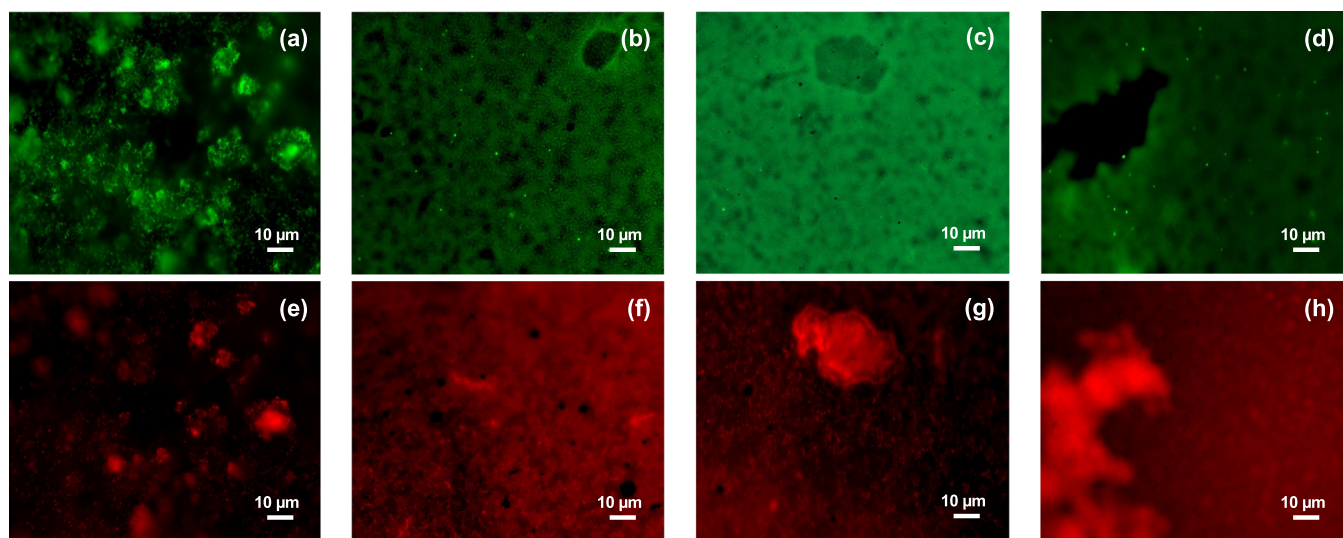


Fig. 6 LIVE/DEAD Biofilm imaging of polyurea coatings. **a, e** Pure polyurea, with **b, f** un-TiO₂, **c, g** 3%Ce-doped TiO₂, and **d, h** 3%La-doped TiO₂ in *Pseudomonas* CDC-reactor.

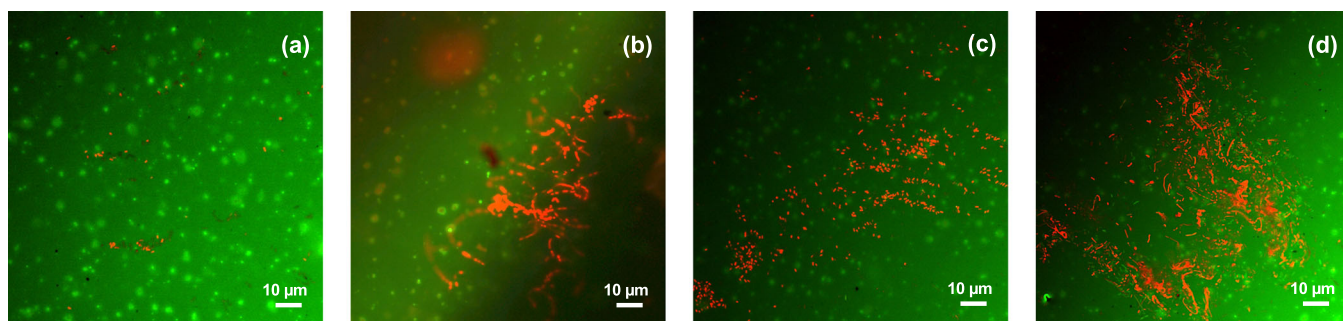


Fig. 7 LIVE/DEAD Biofilm imaging of polyurea coatings. **a** Pure polyurea, with **b** un-TiO₂, **c** 3%Ce-doped TiO₂, and **d** 3%La-doped TiO₂ in *E. coli* CDC-reactor.

observed within the same images, and their unique bactericidal, as well as potentially thermal photocatalytic effects, could be proved. However, how much the nanoparticles, nano-TiO₂ or Ce/La-doped nano-TiO₂, would contribute to the antibacterial effect was under further investigation. And compiling the surface wettability results in Chapter 3.4, it was not difficult to find out the antibiofouling mechanisms for these hydrophilic polyurea coatings: the attachment of microbial cells was raised due to the certain surface roughness caused by the nanoparticles, while the existence of enhanced ROS effect of these Ce/La-doped TiO₂ was the key factor for the antibiofouling performance^{9,27,28}.

Environmental temperature effect on antibacterial activity. Reactive oxygen species (ROS) would be generated by the nano-TiO₂ under the irradiation of the ultraviolet (UV) light, which could damage the cell membrane as well as internal DNA of the biofilm cells, oxidize the fatty acids in lipid, and result in irreversible damage to the cells^{16,28}. With a slight increment of the environment temperature, a slight increase of the colony-forming unit (CFU) within the bioreactor was obtained for the Pure polyurea group, as high temperature might increase the growing and dispersal speed for both *E. coli* and *Pseudomonas*. While for the undoped TiO₂, 3%Ce-doped TiO₂, and 3%La-doped TiO₂ coatings, both CFUs significantly decreased as indicated in Fig. 8a, b. The undoped nano-TiO₂ polyurea indicates low CFU amounts for both cells, i.e., the amount of viable *Pseudomonas* cell (Fig. 8a) decreased from 6.49 log mL⁻¹ at to 5.04 log mL⁻¹ at

20 min for, while the *E. coli* cell (Fig. 8b) reduced from 6.28 log mL⁻¹ to 5.32 log mL⁻¹.

After introducing Ce/La-doped TiO₂ into the polyurea coatings, the bactericidal effects increased greatly with the irradiation time. Compared with the undoped TiO₂ polyurea, it was believed that a more significant bactericidal effect of Ce/La-doped TiO₂ might be obtained as more ROS would generate via the thermal catalytic effect of Ce/La-dopants within the coatings²⁹. For Ce/La-doped TiO₂ polyurea, 3%La-doped TiO₂ indicated an even higher removal efficiency. The viable *Pseudomonas* cell decreased from 6.43 log mL⁻¹ to 4.96 log mL⁻¹, whereas the *E. coli* cell reduced from 6.35 log mL⁻¹ to 4.90 log mL⁻¹. To conclude, the high temperature might contribute to the catalytic effect, caused by the Ce/La-dopants and ended up with the higher degradation of the biofilm compared with Pure polyurea with the absence of nano-TiO₂.

Quorum sensing (QS) is normally used to describe the ability of bacteria to sense and respond to changes in cell density via various regulations^{30,31}. It is believed that the bacteria transport and cell communications would significantly increase at high temperatures and more planktonic *Pseudomonas* and *E. coli* cells might have a reversible and irreversible attachment on the polyurea coating surface. Other than *Pseudomonas*, which can produce AHLs (gram negative QS signalling molecule) for cell communication, bacteria such as *E. coli* and *Salmonella* that do not produce AHLs it still possesses AHL response regulator protein, enabling it to respond to AHLs made by other bacteria. However, the reduction of CFU amounts for both cells as well as the leaking

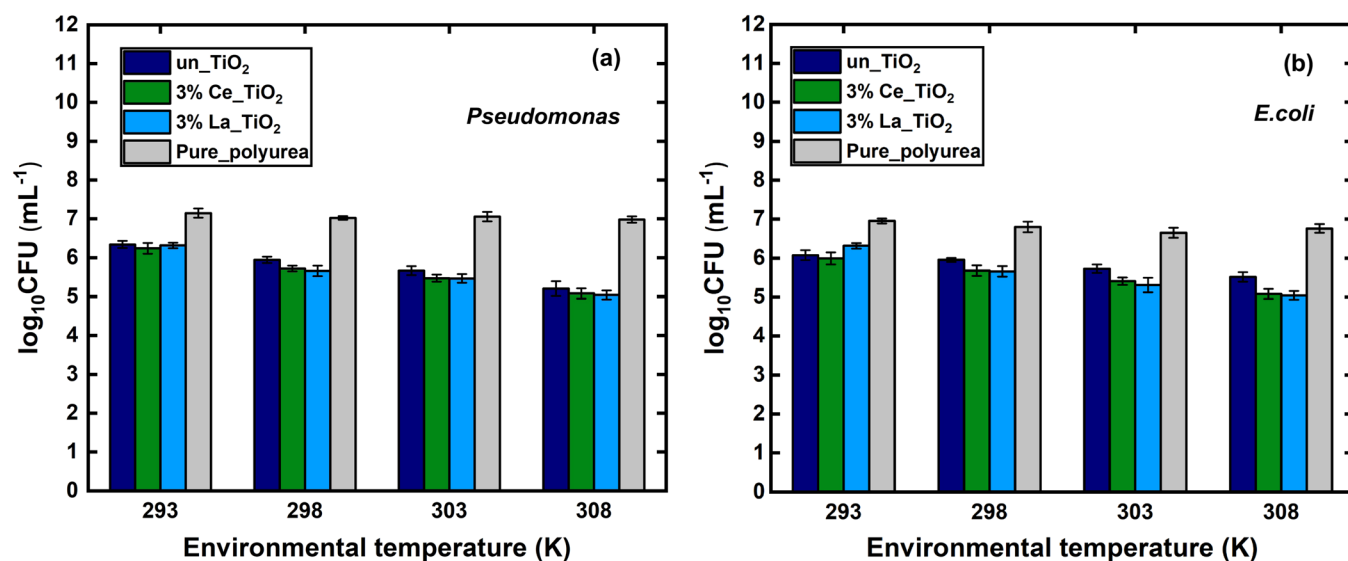


Fig. 8 Increment of antibacterial effect with different temperature within different biofilm reactors. **a** *E. coli* CDC-reactor and **b** *Pseudomonas* CDC-reactor & Increment of antibacterial effect with higher environmental temperatures within *E. coli* CDC-reactor and *Pseudomonas* CDC-reactor.

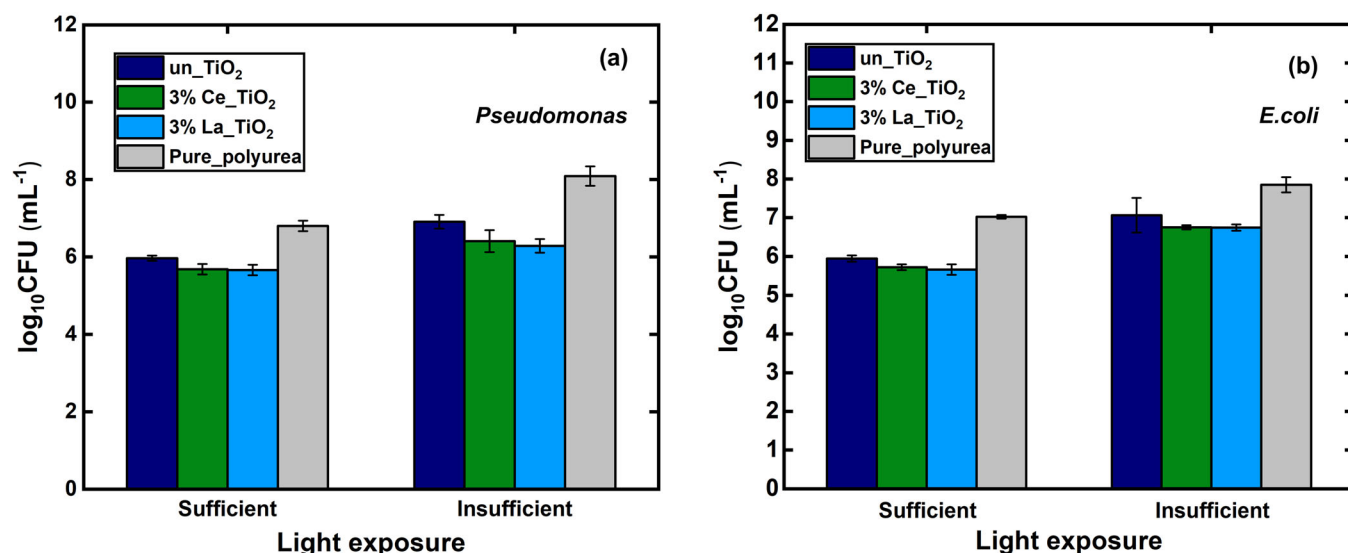


Fig. 9 Increment of antibacterial effect with different light exposure within different biofilm reactors. **a** *E. coli* CDC-reactor and **b** *Pseudomonas* CDC-reactor & Increment of antibacterial effect with higher environmental temperatures within *E. coli* CDC-reactor and *Pseudomonas* CDC-reactor.

signal molecules which was stained in brightly red or green demonstrated that the introduction of undoped nano-TiO₂ and Ce/La-doped TiO₂ in the polyurea coating would influence the quorum sensing/quench among these cells. Such quorum quenching effect might also disturb the communication, cause signal molecule degradation and signal reception disruption, and regulate the production of virulence factors, including extracellular enzymes and cellular lysins^{28,31}.

Light exposure effect on antibacterial activity. In Fig. 9a, b, the effect of different light exposure levels and comparisons on their antibacterial activity could also be exhibited in the bar charts. All doped polyurea coatings could have greater *Pseudomonas* and *E. coli* removal effects at insufficient light exposure levels. The sufficient light exposure result remained the same as 298 K and 20 min exposure as shown in Fig. 8, while the insufficient

condition was also included in Fig. 9 to demonstrate the effect of Ce/La-dopants on antibacterial activities. In the *Pseudomonas* and *E. coli* CDC-reactor, the CFU amount for undoped-TiO₂ polyurea became as low as 6.76 log mL⁻¹ and 6.71 log mL⁻¹, respectively, while the control group Pure_polyurea coating raised as high as 8.05 log mL⁻¹ and 8.48 log mL⁻¹ after 20 min insufficient light exposure at 293 K. The 3%Ce-doped TiO₂ and 3%La-doped TiO₂ coatings almost remained the same level of CFU amounts at 6.75 log mL⁻¹ and 6.36 log mL⁻¹ for *Pseudomonas* and *E. coli* respectively. Both Ce/La-doped nano-TiO₂ coating groups illustrated a greater bactericidal effect than the undoped TiO₂ under insufficient light conditions. These results might also be supported for the hypothesis that, other than the photocatalytic activity generated by nano-TiO₂ via UV excitation, the thermal catalytic effect of the Ce/La-dopants would also help for the generation of a higher concentration of ROS than the original

undoped TiO₂ coatings and the less attachment of both *E. coli* and *Pseudomonas*²⁸. Moreover, it was believed that, under such insufficient light conditions, there would be a more significant decrease of biofilm if the environmental temperature continuously was raised^{30,31}.

The Ce/La doped TiO₂ polyurea coating might be used as the next generation of the antibacterial agent after silver nanoparticles. These rapidly prepared polyurea coatings might also be suited in many other surface areas to improve their antibacterial and anti-viral capabilities (e.g., medical context, frequently touched the surface, and food industry). The antibacterial mechanism of such nano antibacterial material may be related to the immobilization of proteins and enzymes, especially polysaccharides, with the help of Ce/La-doped TiO₂^{26,31}. Although the detachment of both *E. coli* and *Pseudomonas* could prove its feasibility for the practical usage for such polyurea coatings, more bacteria or even viruses were supposed to be tested and studied soon.

METHODS

Synthesis of Ce/La-doped nano-TiO₂

The nano-TiO₂ was prepared by liquid-phase method described in the literature^{10,11}. The solution was centrifuged, and the pellet was washed with deionized water and absolute ethanol 5–6 times. Then Cerium (II) nitrate hexahydrate (Ce(NO₃)₃ · 6H₂O) and Lanthanum (III) oxide (La₂O₃) (Sigma Aldrich, Bangkok, Thailand) were dissolved together using the appropriate 15 wt.% nitric acid with the precipitate at solution pH 7.2. Finally, the mixture solution was stirred at 85 °C for 0.5 h at 1200 rpm and sonicated using a KQ-400DB CNC ultrasonic cleaning machine (Orioner, KL, Malaysia). After dehydrating under 45 degrees Celsius for 1.5 h, rare-earth-doped nano-TiO₂ was obtained¹². The doping amount of rare-earth element was 3.0 wt.% of the mass weight of TiO₂. Diethanolamine purity (purity 99%), glacial acetic acid (purity 99.5%), other chemicals were at least analytical reagent grade and were purchased from Sigma Aldrich.

Preparation of polyurea coatings with Ce/La-doped nano-TiO₂

50–80 wt.% isocyanates (TDI) and 50–90 wt.% polyether amines (Polyoxypropylenediamine)^{7,13} of Brand Dragonshield-BC™ (Washington, DC, USA) were used to fabricate polyurea coating system. 3.0 wt.% of Ce/La-doped nano-TiO₂ within the coating system was proposed for the ideal preparations. The coating group with and without Ce/La-doped nano-TiO₂ were named un-TiO₂, 3%Ce-TiO₂, and 3%La-TiO₂ respectively. Another control group of pure polyurea coating was also fabricated, which was named after Pure_Polyurea. Still, 1.5 wt.% of polydimethylsiloxane (PDMS) was selected for all formula groups as the deforming agent. Polyurea coating was mixed, with a vacuum level of 0.5 kPa, by Kakuhunter SK-300TVSII mixer (Shashin Kagaku Pte Ltd, Japan) at 70 °C for 160 s⁸. The revolution and rotation speed were set at 580 rpm and 1700 rpm, respectively. After mixing, the polyurea was poured into Teflon modes and put into an oven under 70 °C for a curing of 48 h for the following materials characterizations.

Characterization and properties of polyurea coatings

The X-ray diffraction (XRD) measurements were performed by XRD-600 (Shimadzu, Tokyo, Japan). The morphology of the materials was studied by scanning electron microscopy (SEM) using a JEOL microscope (JSM-6510-LV, JEOL, Tokyo, Japan) and by a transmission electron microscopy (TEM) using a JEOL JEM 3010 (300 kV) microscope (JEOL, Massachusetts, USA)¹⁴. The tensile and flexural properties of the nanocomposites were measured using a AGS-J (SHIMADZU/SSL, Shanghai, China). The tests were performed as per ASTM: D638 and ASTM: D790-10 methods, respectively. A cylindrical cutter with 6 mm inner diameter compressed with a hydronic compressor via the same equipment was used to prepare specimens for compression tests. ASTM-D-2240-00 Type A Teclock durometer (Shenzhen, China) was used to test the hardness and its impact resistance and durability. High resolution spectra were collected using 25 eV at 0.1 eV steps with a chamber pressure below 7.5 × 10^{−9} mbar. Five images were taken for each surface at a working distance of 7 mm and a potential of 5 kV. Moreover, the surface profiling for the surface roughness (R_a) was measured by

Alpha-Step D-500 stylus profiler (KLA-Tencor, Milpitas, California, CA, US). Besides, static water contact angles (CA) were measured with distilled water using the sessile drop method by Contact Angle System OCA15 plus (Data physics, Germany). Surface energy (SFE) measurements were made in triplicate for three groups of samples in each series at room temperature, followed the standard operating procedure as documented^{16,17}. Surface energy was measured using three different liquids, diiodomethane, ethylene glycol, and distilled water with a volume of 0.7 µL and a dose rate of 0.1 µL/min (diiodomethane) and volume of 2.0 µL and a dose rate of 0.1 µL/min (ethylene glycol) at room temperature, respectively. Data were analyzed by SCA 20 software (Data physics, Germany) from its regression line. The UV-Vis absorption and reflectance spectrums of the various coatings were investigated with diffuse reflectance (DR) UV-visible (UV-Vis) spectroscopy using an Agilent Cary 5000 spectrophotometer (Cary, California, USA), coupled with an integration sphere for diffuse reflectance studies (DRS), using a Carywin-UV/scan software^{15,16}. And this spectra was also served as a pre-validation work regarding the mechanism of the antibacterial activity due to the photocatalytic factor for the bioassays sector as below.

Experimental measurement of antibacterial activities

For the antimicrobial evaluations, colonies of *Escherichia coli* (*E. coli*, gram-negative, 8099) and *Pseudomonas aeruginosa* isolated from the local drinking water distribution system were used for antibacterial activity assessment by CDC biofilm reactor (BioSurface Technologies Corp., Bozeman, Montana, USA). The bacterium was cultured in a nutrient-rich distilled water medium under the ambient temperature of an average 25 degrees Celsius, 105 kPa for 20 min. Cultures in the nutrient media was diluted to 0.05 OD600 in distilled water, then cultured for 24 h under ambient temperature, at 150 rpm stirring speed, with a batch reactor setup. The source of UV-irradiation remained the same as previous bioassays^{15,16}. Coupons were collected after 5, 10, 15, 20, and 25 min of exposure, and comparison in between different environmental temperature (20, 25, 30, and 35 degrees Celsius) and different light exposure conditions with one half-shaded from UV irradiation (Insufficient condition) and another exposed to ambient light (Sufficient condition) were performed. The biofilms on the smooth side of the coating were stained with the FilmTracer LIVE/DEAD Biofilm Viability Kit (Thermo Fisher Scientific, Waltham, MA, US). Imaging was performed using the Carl Zeiss LSM 780 laser scanning confocal microscope (Zeiss, Jena, Germany)¹⁶. The error bar in Fig. 8 and Fig. 9 is based on the value of mean ± standard deviation (Mean ± SD). Besides, all the *p*-value as summarized from both figures for the bacterial strains statistical significances were also confirmed to be less than 5% for all the bioassays results.

DATA AVAILABILITY

The data that support the findings of this study are available from the corresponding author upon reasonable request.

Received: 3 February 2022; Accepted: 10 April 2022;

Published online: 12 May 2022

REFERENCES

- Choi, K.-M., An, H.-C. & Kim, K.-S. Identifying the hazard characteristics of powder byproducts generated from semiconductor fabrication processes. *J. Occup. Environ. Hyg.* **12**, 114–122 (2015).
- Sung, J.-H. et al. Application of powdered activated carbon coating to fabrics in a hybrid filter to enhance mercury removal. *J. Environ. Sci.* **80**, 58–65 (2019).
- Li, Y., Liu, Y., Yao, B., Narasimalu, S. & Dong, Z. Rapid preparation and anti-microbial activity of polyurea coatings with RE-Doped nano-ZnO. *Microb. Biotechnol.* **15**, 548–560 (2022).
- Z814 One Minute Putty Fast-curing Steel Filled 2 Component Epoxy Putty Of Extremely High Bond Strength For Emergency Leak Sealing 1:1 Mixing 2-3 Minuts Pot Life Ideal For Emergency Repairs In 24 MI Syringe Pack Of Stanvac Chemicals Or Superon Schweisstech", *Mena Report* (2017).
- Chattopadhyay, D. & Raju, K. V. S. Structural engineering of polyurethane coatings for high performance applications. *Prog. Polym. Sci.* **32**, 352–418 (2007).
- Holm, E. R. et al. Interspecific variation in patterns of adhesion of marine fouling to silicone surfaces. *Biofouling* **22**, 233–243 (2006).

7. Li, Y., Luo, B., Guet, C., Narasimalu, S. & Dong, Z. Preparation and formula analysis of anti-biofouling titania-polyurea spray coating with nano/micro-structure. *Coatings* **9**, 560 (2019).
8. Li, Y., Woo, Y., Sekar, M., Narasimalu, S. & Dong, Z. Effect of nano-titanium dioxide contained in titania-polyurea coating on marina biofouling and drag reduction. *J. Biomed. Nanotechnol.* **16**, 1530 (2020).
9. Wang, J. et al. Simultaneous removal of graphene oxide and chromium(VI) on the rare earth doped titanium dioxide coated carbon sphere composites, *ACS Sustain. Chem. Eng.* **5**, 5550–5561 (2017).
10. Fu, L., Hamzeh, M., Dodard, S., Zhao, Y. H. & Sunahara, G. I. Effects of TiO₂ nanoparticles on ROS production and growth inhibition using freshwater green algae pre-exposed to UV irradiation. *Environ. Toxicol. Pharm.* **39**, 1074–1080 (2015).
11. Kim, C.-H., Lee, E.-S., Kang, S.-M., de Josselin de Jong, E. & Kim, B.-I. Bactericidal effect of the photocatalytic reaction of titanium dioxide using visible wave-lengths on *Streptococcus mutans* biofilm. *Photodiagnosis Photodyn. Ther.* **18**, 279–283 (2017).
12. Farha, M. A. & Brown, E. D. Discovery of antibiotic adjuvants: modeling the production of reactive oxygen species in bacteria reveals targets for adjuvants that boost antibiotic activity. *Nat. Biotechnol.* **31**, 120 (2013).
13. Cattò, C., Villa, F. & Cappitelli, F. Recent progress in bio-inspired biofilm-resistant polymeric surfaces. *Crit. Rev. Microbiol.* **44**, 633–652 (2018).
14. Deng, Y.-J., Lu, Y., Liu, J.-K. & Yang, X.-H. Production and photoelectric activity of P and Al Co-Doped ZnO nanomaterials. *Eur. J. Inorg. Chem.* **2015**, 3708–3714 (2015).
15. Li, L. et al. Mid-temperature deep removal of hydrogen sulfide on rare earth (RE=Ce, La, Sm, Gd) doped ZnO supported on KIT-6: Effect of RE dopants and interaction between active phase and support matrix. *Appl. Surf. Sci.* **407**, 197–208 (2017).
16. Honglin, L., Yingbo, L., Jinzhu, L. & Ke, Y. Experimental and first-principles studies of structural and optical properties of rare earth (RE = La, Er, Nd) doped ZnO. *J. Alloy. Compd.* **617**, 102–107 (2014).
17. Reséndiz López, E. et al. Bandgap modification of titanium dioxide doped with rare earth ions for luminescent processes. *Int. J. Appl. Phys.* **128**, 175106 (2020).
18. Bao, R. et al. Effects of rare earth elements and nitrogen Co-doped on the photocatalytic performance of TiO₂. *Cryst. Res. Technol.* (1979) **53**, 1700138 (2018).
19. Bhethanabotla, V. C., Russell, D. R. & Kuhn, J. N. Assessment of mechanisms for enhanced performance of Yb/Er/titania photocatalysts for organic degradation: Role of rare earth elements in the titania phase. *Appl. Catal. B* **202**, 156–164 (2016).
20. Xie, K., Jia, Q., Wang, Y., Zhang, W. & Xu, J. The electronic structure and optical properties of anatase TiO₂ with rare earth metal dopants from first-principles calculations. *Materials* **11**, 179 (2018).
21. Gong, P. et al. Syntheses, structural characterization and photophysical properties of two series of rare-earth-isonicotinic-acid containing Waugh-type manganomolybdates. *Cryst. Eng. Comm.* **19**, 834–852 (2017).
22. ASTM: D638 Standard Test Method for Tensile Properties of Plastics
23. ASTM: D790-10 Standard Test Methods for Flexural Properties
24. ASTM-D-2240-00 Standard Test Method for Rubber Property
25. Yuan, S. & Pehkonen, S. Pulsed ultraviolet light inactivation of pseudomonas aeruginosa and staphylococcus aureus biofilms: Pulsed UV inactivation of microbial biofilms. *Colloids Surf. B* **59**, 87–99 (2007).
26. Desch, A. et al. Biofilm formation on zirconia and titanium over time—An in vivo model study. *Clin. Oral. Implants Res.* **31**, 865–880 (2020).
27. Gustumhaugen, E. et al. Effect of chemical and mechanical debridement techniques on bacterial re-growth on rough titanium surfaces: an in vitro study. *Clin. Oral. Implants Res.* **25**, 707–713 (2014).
28. Dworniczek, E. et al. Photo-catalytic inactivation of an Enterococcus biofilm: the anti-microbial effect of sulphated and europium-doped titanium dioxide nanoparticles. *FEMS Microbiol. Lett.* **363**, fnw051 (2016).
29. Arango-Santander, S., Pelaez-Vargas, A., Freitas, S. C. & García, C. A novel approach to create an antibacterial surface using titanium dioxide and a

combination of dip-pen nanolithography and soft lithography. *Sci. Rep.* **8**, 15818–10 (2018).

30. Lopes, F. et al. Biomaterialized diamond-like carbon films with incorporated titanium dioxide nanoparticles improved bioactivity properties and reduced biofilm formation. *Mater. Sci. Eng. C* **81**, 373–379 (2017).
31. Li, Y., Xiao, P., Wang, Y. & Hao, Y. Mechanisms and control measures of mature biofilm resistance to antimicrobial agents in the clinical context. *ACS Omega* **5**, 22684–22690 (2020).

ACKNOWLEDGEMENTS

This research was funded by MOE Academic Research Fund (AcRF) Tier 1 Project “Nano-structured Titania with tunable hydrophilic/hydrophobic behaviour and photocatalytic function for marine structure application”, Grant Call (Call 1/2018) _MSE (EP Code EP5P, Project ID 122018-T1-001-077), Ministry of Education (MOE), Singapore.

AUTHOR CONTRIBUTIONS

Authors contribution: Cong Fang is also the co-first author of this paper. Yuanzhe Li and Cong Fang make substantial contributions to the conception and design of the work and the acquisition; Yuanzhe Li and Haojing Wang greatly contribute to the analysis and interpretation of the data; Yuanzhe Li and Cong Fang draft the work; Weiqin Zhuang and Xueli Wang revise it critically for important intellectual content; Yuanzhe Li and Cong Fang make the final approval of the completed version; Xueli Wang takes the accountability for all aspects of the work in ensuring that questions related to the accuracy or integrity of any part of the work are appropriately investigated and resolved; Haojing Wang is in charge of visualization of the biochemical diagrams as well as formatting of the work.

COMPETING INTERESTS

The authors declare no competing interests.

ADDITIONAL INFORMATION

Correspondence and requests for materials should be addressed to Xueli Wang.

Reprints and permission information is available at <http://www.nature.com/reprints>

Publisher's note Springer Nature remains neutral with regard to jurisdictional claims in published maps and institutional affiliations.



Open Access This article is licensed under a Creative Commons Attribution 4.0 International License, which permits use, sharing, adaptation, distribution and reproduction in any medium or format, as long as you give appropriate credit to the original author(s) and the source, provide a link to the Creative Commons license, and indicate if changes were made. The images or other third party material in this article are included in the article's Creative Commons license, unless indicated otherwise in a credit line to the material. If material is not included in the article's Creative Commons license and your intended use is not permitted by statutory regulation or exceeds the permitted use, you will need to obtain permission directly from the copyright holder. To view a copy of this license, visit <http://creativecommons.org/licenses/by/4.0/>.

© The Author(s) 2022